Enhanced Structural and Optical Properties of Pr^{3+}Substituted Gadolinium Garnet Ferrite for Optical Devices Application

Anjori Sharma and Dipesh

1 Introduction

The importance of ferrites is increasing day by day. The reason is its uncountable applications, which increase its demand for new technologies [1–5]. Ferrites are known for excellent magnetic, insulating, structural stability, optical, optoelectrical, and dielectric properties. Due to good properties, ferrites are used in communication device, memory devices, optical storage, microwave absorption, antenna applications, and many more [6–11].

Ferrites are ceramic oxides that are categorized into three types: hexagonal ferrites, garnet ferrites, and spinel ferrites. All the ferrites have their own individual properties. Spinel ferrites and garnet ferrites are cubic in structure. Hexagonal ferrites have hexagonal structure. Garnet ferrites are superior than other ferrites because spinel ferrites are limited in high frequency region. Whereas hexagonal ferrites required higher preparation temperature. Due to very good dielectric, optical, magnetic, thermal, electromagnetic, and low losses [12–15], garnet ferrites are more fascinating nowadays. Garnet ferrites are used in communication devices, microwave devices, optical devices, antennas, optical isolators, and microwave absorption [16, 17]. Factors like sintering temperature, composition, morphology, preparation methods, and other factors affect the properties of ferrites. $R_3Fe_5O_{12}$ is the standard formula for iron garnets, whereby R is rare earth. Garnet ferrites have a cubic crystal structure with the Ia3d space group, and their magnetic characteristics depend on the presence of iron and rare earth cations. In garnet ferrites, there are three sites: dodecahedral site 24c, which is the largest and is occupied by the rare earth ion R^{3+}, octahedral site

A. Sharma (✉)
Department of Physics, Lovely Professional University, Phagwara, Punjab, India
e-mail: anjori.sharma1995@gmail.com

Dipesh
Department of Mathematics, Lovely Professional University, Phagwara, Punjab, India

S. B. Krupanidhi et al. (eds.), *Recent Advances in Functional Materials and Devices*,
Springer Proceedings in Materials 37, https://doi.org/10.1007/978-981-99-6766-7_16

16a, which is occupied by iron ion [Fe^{3+}], and tetrahedral site 24d, which is occupied by iron ion (Fe^{3+}).

Garnet ferrites can be synthesized in a variety of ways. Ball milling is a process that requires a very high temperature; it is extensively utilized, but it has a disadvantage in the form of product inhomogeneity. Many researchers are interested in the hydrothermal technique because it provides a fast rate of heating and efficient reaction kinetics, resulting in a high yield. Another interesting method is the sol—gel method, which provides higher uniformity in the garnet phase due to the rate of mixing, however, this process is limited by the longer time required to dry the gel. Furthermore, the sol—gel auto-combustion method is superior because it solves the problem of gel drying by using a fuel such as citric acid. Substitution can improve the characteristics properties of garnet ferrites. Scandium replacement in the octahedral position increases magnetic properties, while aluminum and gallium substitution in the tetrahedral site decreases it. The use of non-magnetic aluminum instead of magnetic iron ion in YIG alert structural and magnetic properties.

Large number of researches have been carried out on the effect of composition and substitution variation on garnet ferrites. Akhtar et al. [18] have observed that by Cerium (Ce^{3+}) substitution in GdIG, the crystallite size decreases. Yousaf et al. [14] have examined that with substitution of samarium [Sm^{3+}] in YIG the variation in band gap from 1.7 electron Volt to 1.88 electron Volt has been noticed. A. Sharma et al. [19] have examined the influence of substitution of yttrium [Y^{3+}], bismuth [Bi^{3+}], lanthanum [La^{3+}] on GdIG and found that crystallite size varies with substitution. Also, they found that with variation of substitution content, band gap value differs from 3.7 eV to 3.9 eV. M.N. Akhtar [21] has observed that lattice constant does not vary with incorporation of cerium [Ce^{3+}] in GdIG whereas particle size lies between 80–98 nm. M.R. Khalief et al. [20] have examined the influence of Dy^{3+} on Ce^{3+}, Bi^{3+} substitution on YIG. They found that all the prepared samples had impurity of CeO_2.

From the above discussion, it has been found that substitution in garnet ferrites can alert the properties. The motive of this research is to explore the influence of new substitution on GdIG for better structural as well as optical properties. By best of the knowledge no work is done on substitution of praseodymium (Pr^{3+}) in GdIG ($Pr_xGd_{3-x}Fe_5O_{12}$ for x = 0.5, 1.0, and 1.5).

2 Materials and Method

Praseodymium doped Gadolinium iron garnet ($Pr_xGd_{3-x}Fe_5O_{12}$ for x = 0.5, 1.0 and 1.5) was prepared using sol—gel auto-combustion method. Gadolinium (III) nitrate [Gd $(NO_3)_3.6H_2O$], ferric (III) nitrate [Fe $(NO_3)_3$. $6H_2O$], Praseodymium (III) nitrate [Pr $(NO_3)_3$. $6H_2O$] and citric acid ($C_6H_8O_7.H_2O$) of AR grade were used as precursors. The precursors were weighed according to stoichiometric formula and added into 100 ml of distilled water. The formation of garnet ferrite according to stoichiometric ratio is mentioned in the equation below:

$$3Gd\,(NO_3)_3 \cdot 6H_2O + 3Fe\,(NO_3)_3 \cdot 6H_2O + x\,Pr_3(NO_3)_3 \cdot 6H_2O \rightarrow Pr_xGd_{3-x}Fe_5O_{12}$$

The solutions were kept for stirring for thirty minutes in order to form clear solution. In order to maintain the pH approximately 7, ammonia solution was added into the solutions with constant stirring. Then the solution kept for stirring and heating until the gel form. After that, heat is increased to $200-250^{\circ}$ C until gel swells up and auto-combustion reactions start. Finally, powders were obtained after proper drying of samples. These obtained samples were finely ground. The obtained powder was sintered in muffle furnace for 6 h at 1200 ° C temperature.

The phase formation in the praseodymium substituted garnet ferrite ($Pr_xGd_{3-x}Fe_5O_{12}$ for x = 0.5, 1.0, and 1.5) was examined with X-ray diffraction (XRD) spectroscopy of Bruker D8 Advance company. The morphological properties were investigated by field emission scanning electron microscope (FESEM) of JEOL JSM-7610F Plus. The optical features were examined with ultra-violet visible spectroscopy (UV—Vis) of Shimadzu UV—vis 1800 spectrophotometer and fluorescence spectroscopy.

3 Results and Discussions

3.1 Structural Analysis

With X-ray diffraction pattern the structural properties of praseodymium substituted gadolinium iron garnet ($Pr_xGd_{3-x}Fe_5O_{12}$ for x = 0.5, 1.0, and 1.5) were evaluated. Figure 1 represents the XRD pattern of $Pr_xGd_{3-x}Fe_5O_{12}$ (x = 0.5,1 .0, 1.5 represented by PrG1, PrG2, and PrG3, respectively). The diffraction patterns of prepared samples concluded that the gadolinium iron garnet (GdIG) phase is dominating over other phases. The obtained results of the samples were further compared with JCPDS no. 72–0141 of pure GdIG. The cubic structure of prepared samples with space group Ia3d has been assured by miller indices values at (321), (400), (420), (422), (521), (532), (444), (640), (642), (800), (840), (842), and (664) [21]. With more addition of Pr in samples, i.e., from x = 0.5 to 1.5 the impurity phase (Fe_2O_3) has been observed. This impurity phase is due to stoichiometric modification in dodecahedral site [22]. Also, the higher intense peak (420) became less sharp with increase in Pr content in samples. This implies that the sample is becoming less crystalline with higher substitution of Pr. The crystallite size for the samples has been calculated using Debye Scherer Method (Eq. 1) [23].

$$D = \frac{k\lambda}{\beta cos\theta} \tag{1}$$

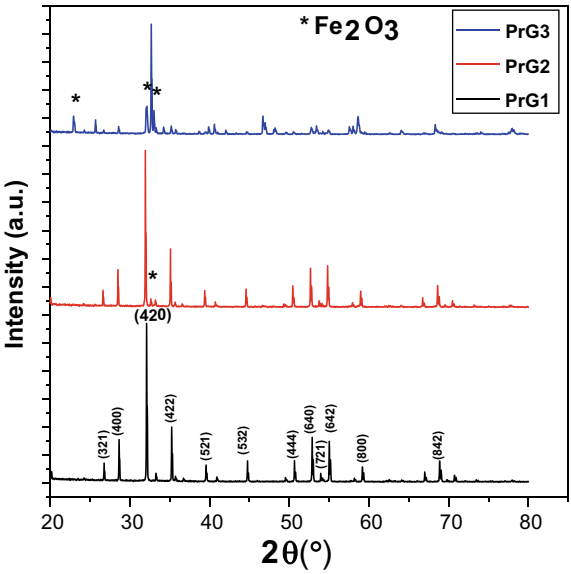

Fig. 1 XRD pattern of PrxGd3-xFe5O12 **a** x = 0.5, **b** 1.0, and **c** 1.5

Here k, λ, β, and θ represent Scherer constant (0.9), X-ray wavelength (0.15406 nm), Full width half maxima (FWHM) and peak position, respectively.

The calculated value of crystallite size "D," lattice constant "a," microstrain "ε" and dislocation density "δ" is tabulated in Table 1. It has been examined that the crystallite size decreases with increase in Pr substitution. The variation in crystallite size with substitution is due to presence of impurities. These impurities further affect the growth of crystal [24]. Second reason of variation can be stress and strain due to Pr substitution which produces defect in lattice [21].

The morphology of Pr substituted samples was examined by the micrographs obtained from FESEM. Figure 2a–c represents the micrographs of the sample PrG1, PrG2, and PrG3. From the deep analysis of micrographs, it can be concluded that all the samples contain spherically shaped grains which is in accordance with literature

Table 1 Calculated values of structural parameters: 2 θ, β, D, a, ε, δ for prepared compositions

Sample	Sample code	2θ(°)	β	hkl	D(nm)	a (Å)	ε (10^{-3})	δ (nm^{-2})
$Pr_xGd_{3-x}Fe_5O_{12}$ (x = 0.5)	PrG1	32.12	0.15	420	52.8	12.45	2.7	0.35
$Pr_xGd_{3-x}Fe_5O_{12}$ (x = 1.0)	PrG2	31.90	0.17	420	46.6	12.51	2.6	0.46
$Pr_xGd_{3-x}Fe_5O_{12}$ (x = 1.5)	PrG3	32.70	0.18	420	44.1	12.23	2.8	0.51

[21]. With increase in Pr^{3+}substitution, agglomeration has been observed. Figure 2a–c represents size distribution histogram of the samples. The large number of grains are obtained at 0.71 μm, 1.1 μm, 77 nm for PrG1, PrG2, and PrG3 sample, respectively.

Line intercept method (Eq. 2) [25] was used to calculate the grain size and tabulated in Table 2.

$$grain\ size = \frac{1.5L}{mn} \tag{2}$$

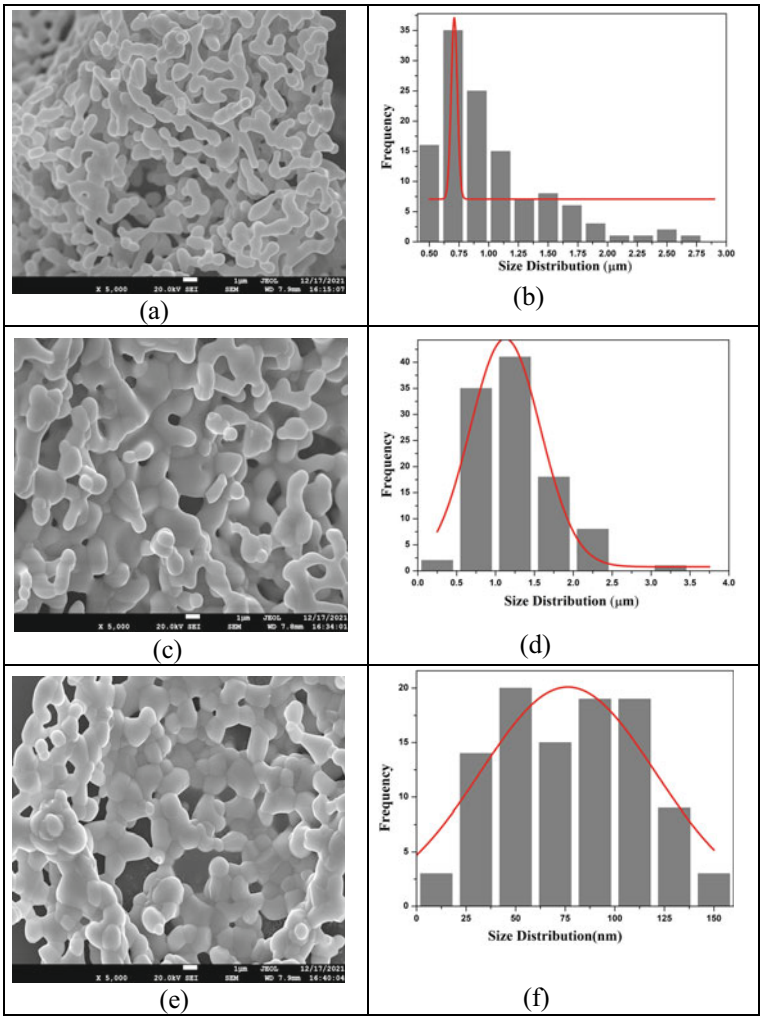

Fig. 2 Micrographs of samples **a** PrG1, **c** PrG2, **e** PrG3 and Gaussian fitted histograms (**b**) PrG1 **b** PrG2 **f** PrG3

Table 2 Calculated grain size of **a** PrG1, **b** PrG2, **c** PrG3

Sample	Grain size (μm)
PrG3	0.308
PrG1	0.271
PrG2	0.401

Here L, m, n represent the line length, magnification mentioned in micrographs, number of grain's intersepts respectively.

The ionic radii of substituted element, temperature, porosity, and method of preparations affect the grain size of the samples [28].

Optical Properties Analysis

The optical properties of the materials depend upon many factors but energy band gap (Eg) and absorption coefficient (α) are very crucial features. These features decide the importance of ferrites for optoelectronic devices. UV—Vis spectroscopy was used to study optical property of $Pr_xGd_{3-x}Fe_5O_{12}$. Figure 3 represents the absorption versus wavelength graph for samples PrG1, PrG2, and PrG3. The absorbance in all samples has been observed up to 280 nm, after that samples show transmittance. A shift in absorbance has been noticed with a change in composition from x = 0.5 to 1.5. The absorbance in the materials depends upon factors like energy band and uneven surface [26]. Figure 4a–c represents $(\alpha h\nu)^2$ versus $(h\nu)$ graphs which are plotted to calculate band gap of the samples. It has been observed that band gap of sample $Pr_xGd_{3-x}Fe_5O_{12}$ first decreases from 4.6 eV to 4.5 eV for x = 0.5 to 1.0. After that, the band gap increases from 4.5 eV to 4.7 eV. The change in bandgap depends upon several factors like crystallite size, impurity, concentration of substituents, and morphology [27].

In order to study the luminescence property and to analyze the energy band gap with related to most strong position of sub band gap fluorescence spectroscopy was studied. Figure 5 represents the fluorescence spectroscopy of $Pr_xGd_{3-x}Fe_5O_{12}$ sample. The excitation wavelength is around 270 nm which is chosen from the obtained UV spectroscopy. At this excitation wavelength it has been observed that

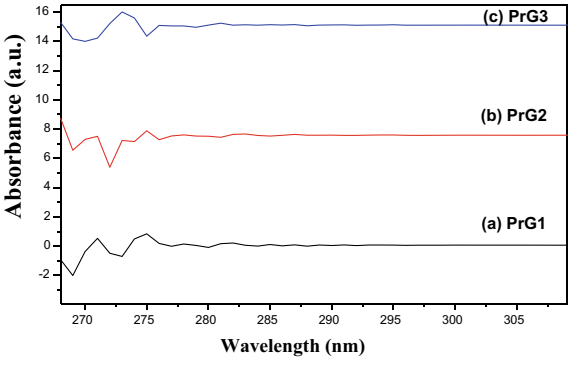

Fig. 3 Absorbance versus wavelength spectra of PrxGd3-xFe5O12 **a** PrG1 **b** PrG2 and **c** PrG3

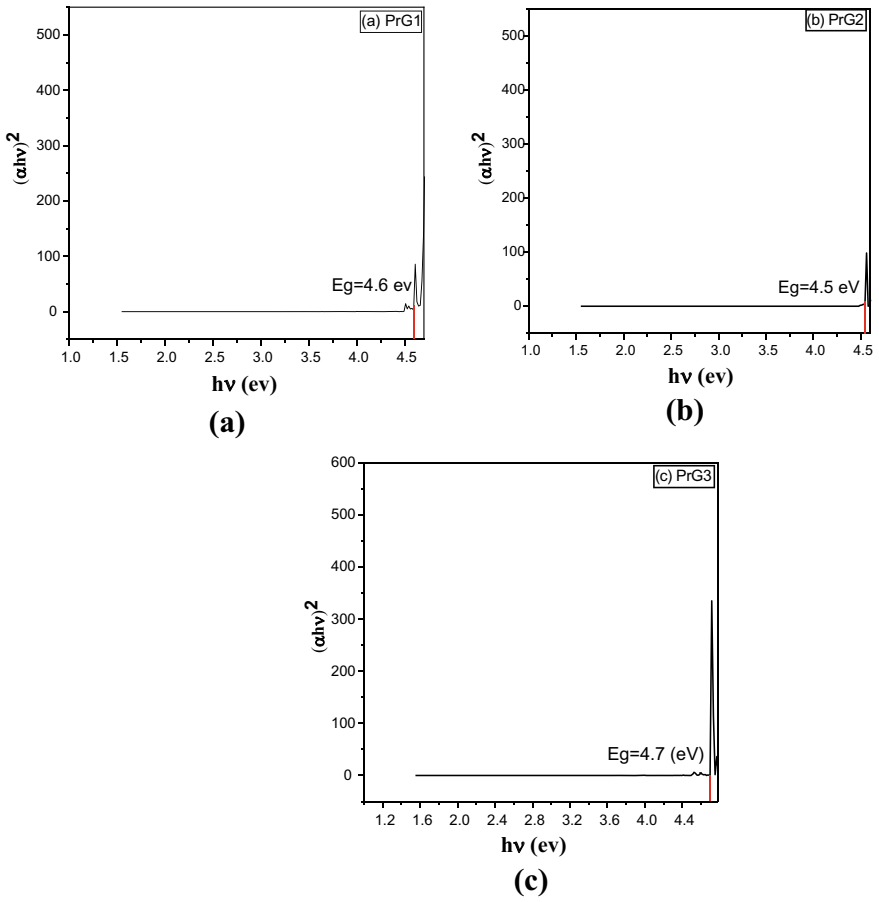

Fig. 4 Calculated band gap of PrxGd3-xFe5O12 **a** PrG1 **b** PrG2 and **c** PrG3

all three samples emit red color, i.e., at 650 nm region. The reason of such emission is presence of nitrates group in prepared samples [26]. A shift has been observed with increases in Pr concentration in $Pr_xGd_{3-x}Fe_5O_{12}$. The intensity of the sample increases with increase in Pr concentration. The reason of increase in fluorescent intensity is because of increase in distance between GdIG and dopant (Pr) [28]. This implies that increases in concentration of dopant increase the emission property. Such properties of $Pr_xGd_{3-x}Fe_5O_{12}$ make it suitable to be used in optical storage and optical devices.

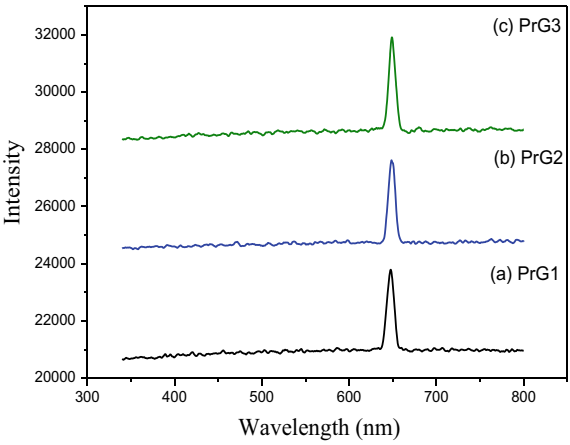

Fig. 5 Fluorescence emission spectra of PrxGd3-xFe5O12 **a** PrG1 **b** PrG2 and **c** PrG3

4 Conclusion

Sol—gel auto-combustion process was carried out to prepare $Pr_xGd_{3-x}Fe_5O_{12}$ for x = 0.5,1.0 and 1.5. XRD confirms the formation of garnet phase in Pr substituted GdIG. It has been observed that with increase in Pr content in garnet ferrite impurity phases were formed. Crystallite size, lattice constant, microstrain and dislocation density also vary with change in Pr content. From FESEM it has been observed that maximum number of grains lies in 0.71 μm, 1.1 μm, 77 nm for x = 0.5, 1.0, and 1.5 sample respectively. The bandgap evaluated from UV—Vis spectra was found in 4.5 eV to 4.7 eV range. From fluorescence spectroscopy it has been found that with increases in concentration of dopant, emission property enhanced.

References

1. Tatarchuk T, Naushad M, Tomaszewska J, Kosobucki P, Myslin M, Vasylyeva H, Ścigalski P (2020) Adsorption of Sr (II) ions and salicylic acid onto magnetic magnesium-zinc ferrites: isotherms and kinetic studies. Environ Sci Pollution Res 27(21):26681–26693
2. Tatarchuk T, Shyichuk A, Sojka Z, Gryboś J, Naushad M, Kotsyubynsky V, Kowalska M, Kwiatkowska-Marks S, Danyliuk N (2021) Green synthesis, structure, cations distribution and bonding characteristics of superparamagnetic cobalt-zinc ferrites nanoparticles for Pb (II) adsorption and magnetic hyperthermia applications. J Molecular Liquids 328:115375
3. Tatarchuk T, Myslin M, Lapchuk I, Shyichuk A, Murthy AP, Gargula R, Kurzydło P, Bogacz BF, Pędziwiatr AT (2021) Magnesium-zinc ferrites as magnetic adsorbents for Cr (VI) and Ni (II) ions removal: cation distribution and antistructure modeling. Chemosphere 270:129414
4. Kozlovskiy AL, Kenzhina IE, Zdorovets MV (2020) FeCo–Fe2CoO4/Co3O4 nanocomposites: Phase transformations as a result of thermal annealing and practical application in catalysis. Ceram Int 46(8):10262–10269
5. Zdorovets MV, Kozlovskiy AL (2020) Study of phase transformations in Co/CoCo2O4 nanowires. J Alloy Compd 815:152450

6. Akhtar MN, Khan MA, Ahmad M, Nazir MS, Imran M, Ali A, Sattar A, Murtaza G (2017) Evaluation of structural, morphological and magnetic properties of CuZnNi (CuxZn0. 5− xNi0. 5Fe2O4) nanocrystalline ferrites for core, switching and MLCI's applications. J Magnet Magnetic Mater 421:260–268
7. Rubinger CPL, Gouveia DX, Nunes JF, Salgueiro CCM, Paiva JAC, Graça MPF, Andre P, Costa LC (2007) Microwave dielectric properties of NiFe2O4 nanoparticles ferrites. Microw Opt Technol Lett 49(6):1341–1343
8. Ravinder D, Reddy P, Shalini P (2003) Frequency and composition dependence of dielectric behavior of copper substituted lithium ferrites. J Mater Sci Lett 22(22):1599–1601
9. Chen W, Dongsheng L, Wenwei W, Huaxin Z, Juan W (2017) Structure and magnetic properties evolution of rod-like Co0. 5Ni0. 25Zn0. 25DyxFe2− xO4 synthesized by solvothermal method. J Magnet Magnetic Mater 422:49–56
10. Jia Z, Misra RDK (2011) Magnetic sensors for data storage: perspective and future outlook. Mater Technol 26(4):191–199
11. Seongatae B, Won LS, Hirukawa A, Takemura Y, Youn J, Haeng GLS (2009) AC magnetic-field-induced healing and physical properties of ferrite nanocomposites for a hyperthermia agent in medicine. IEEE Transactions Nanotechnology 8:86–94
12. Sattar AA, Elsayed HM, Faramawy AM (2016) Comparative study of structure and magnetic properties of micro-and nano-sized GdxY3− xFe5O12 garnet. J Magn Magn Mater 412:172–180
13. Arun T, Vairavel M, Raj SG, Joseyphus RJ (2012) Crystallization kinetics of Nd-substituted yttrium iron garnet prepared through sol–gel auto-combustion method. Ceram Int 38(3):2369–2373
14. Yousaf M, Noor A, Xu S, Akhtar MN, Wang B (2020) Magnetic characteristics and optical band alignments of rare earth (Sm+ 3, Nd+ 3) doped garnet ferrite nanoparticles (NPs). Ceramics International 46(10):16524–16532
15. Praveena K, Srinath S (2014) Effect of Gd3+ on dielectric and magnetic properties of Y3Fe5O12. J Magn Magn Mater 349:45–50
16. Akhtar MN, Sulong AB, Ahmad M, Khan MA, Ali A, Islam MU (2016) Impacts of Gd–Ce on the structural, morphological and magnetic properties of garnet nanocrystalline ferrites synthesized via sol–gel route. J Alloy Compd 660:486–495
17. Kidoh H, Morimoto A, Shimizu T (1991) Synthesis of ferromagnetic Bi-substituted yttrium iron garnet films by laser ablation. Applied physics letters 59(2):237–239
18. Akhtar MN, Kashif A, Umer A, Ahmad T, Khan MA (2018) Structural elucidation, and morphological and magnetic behavior evaluations, of low-temperature sintered, Ce-doped, nanostructured garnet ferrites. Mater Res Bull 101:48–55
19. Sharma A, Godara SK, Srivastava AK (2021) Effect of Y3+, Bi3+, La3+ substitution on structural, optical and magnetic properties of gadolinium iron garnets. Materials Today: Proceedings
21. Akhtar MA, Sulong AB, Ahmad M, Khan MA, Ali A, Islam MU (2016) Impacts of Gd–Ce on the structural, morphological and magnetic properties of garnet nanocrystalline ferrites synthesized via sol–gel route. Journal of Alloys and Compounds 660:486–495
20. Khalifeh MR, Shokrollahi H, Arab SM, Yang H (2020) The role of Dy incorporation in the magnetic behavior and structural characterization of synthetic Ce, Bi-substituted yttrium iron garnet. Mater Chem Phys 247:122838
21. Mohaidat QI, Lataifeh M, Hamasha K, Mahmood SH, Bsoul I, Awawdeh M (2018) The structural and the magnetic properties of aluminum substituted yttrium iron garnet. Materials Research 21.
22. Sharma A, Godara SK, Maji PK, Srivastava AK (2021) Influence of Temperature on Structural and Magnetic Properties of Gd3AlxFe5− xO12 (x= 2). Crystal Research and Technology 2100109
23. Sharma A, Mahajan M, Mohammed I, Sinha S, Godara SK, Srivastava AK (2023) Effect of Sintering Temperature on the Structural, Dielectric, and Magnetic Properties of Garnet-Spinel Ferrite Composites for Use in L-Band Devices. Materials Performance and Characterization 12(1):64–78

24. Basavad M, Shokrollahi H, Ahmadvand H, Arab SM (2020) Structural, magnetic and magneto-optical properties of the bulk and thin film synthesized cerium-and praseodymium-doped yttrium iron garnet. Ceram Int 46(8):12015–12022
25. Sharma A, Mohammed I, Godara SK, Srivastava AK (2022) Low dielectric losses and enhanced magnetic property of ErIG (x)/YIG (1− x) (x= 0.5) composite for antenna applications. Bulletin of Materials Science 45(4): 248
28. Yousaf M, Noor A, Xu S, Akhtar MN, Wang B (2020) Magnetic characteristics and optical band alignments of rare earth (Sm+ 3, Nd+ 3) doped garnet ferrite nanoparticles (NPs). Ceramics International 46(10): 16524–16532
26. Chavan P (2021) Facile Synthesis, Diffused Reflectance Spectroscopy & Fluorescence Studies of Ni0. 5− xMg0. 5CuxFe2O4 Nanoparticles. Journal of Fluorescence 31(4):1023–1028
27. Chavan P, Naik LN, Belavi PB, Chavan GN, Kotnala RK (2017) Synthesis of Bi3+ substituted Ni-Cu ferrites and study of structural, electrical and magnetic properties. Journal of Alloys and Compounds 694:607–612
28. Talukdar S, Rakshit R, Krämer A, Müller FA, Mandal K (2018) Facile surface modification of nickel ferrite nanoparticles for inherent multiple fluorescence and catalytic activities. RSC advances 8(1):38–43